BIOMATERIALS

Bioadhesive polymer semiconductors and transistors for intimate biointerfaces

Nan Li^{1,2}, Yang Li¹, Zhe Cheng², Youdi Liu¹, Yahao Dai¹, Seounghun Kang¹, Songsong Li¹, Naisong Shan¹, Shinya Wai¹, Aidan Ziaja¹, Yunfei Wang³, Joseph Strzalka⁴, Wei Liu¹, Cheng Zhang¹, Xiaodan Gu³, Jeffrey A. Hubbell^{1,5,6}, Bozhi Tian², Sihong Wang^{1,7}*

The use of bioelectronic devices relies on direct contact with soft biotissues. For transistor-type bioelectronic devices, the semiconductors that need to have direct interfacing with biotissues for effective signal transduction do not adhere well with wet tissues, thereby limiting the stability and conformability at the interface. We report a bioadhesive polymer semiconductor through a double-network structure formed by a bioadhesive brush polymer and a redox-active semiconducting polymer. The resulting semiconducting film can form rapid and strong adhesion with wet tissue surfaces together with high charge-carrier mobility of ~1 square centimeter per volt per second, high stretchability, and good biocompatibility. Further fabrication of a fully bioadhesive transistor sensor enabled us to produce high-quality and stable electrophysiological recordings on an isolated rat heart and in vivo rat muscles.

ntegrating biocompatible electronic devices with living biological tissues is emerging as a promising avenue for achieving the real-time measurement of biological signals with high spatiotemporal resolutions for biological studies and health monitoring (1-3). An overarching goal for the development of bioelectronic devices is to achieve conformable and stable interfacing between the sensing surface and the tissue (4-6). This requires soft and stretchable properties on devices for adapting to curvilinear tissue surfaces, combined with stable bonding between the electrical sensing surface and the tissue. Progress has been made in the development of stretchable bioelectronic materials and devices (7-12). However, for interface bonding (13) that necessitates the adhesion property of electronic materials to wet tissue surfaces, successes have been limited to conductors (14-17), which can only be used for passive sensing that has moderate sensitivity.

To realize higher sensitivity, transistor-based active sensing devices are the more advanced option that can provide built-in amplification (18, 19). For biointerfaced sensing, organic electrochemical transistors (OECTs) (20–23) based on semiconducting polymers (Fig. 1A) are one of the more promising options with several advantages, including high amplifi-

¹Pritzker School of Molecular Engineering, The University of Chicago, Chicago, IL 60637, USA. ²Department of Chemistry, The University of Chicago, Chicago, IL 60637, USA. ³School of Polymer Science and Engineering, University of Southern Mississippi, Hattiesburg, MS 39406, USA. ⁴X-Ray Science Division, Argonne National Laboratory, Lemont, IL 60439, USA. ⁵Committee on Immunology, The University of Chicago, Chicago, IL 60637, USA. ⁶Committee on Cancer Biology, The University of Chicago, Chicago, IL 60637, USA. ⁷Nanoscience and Technology Division and Center for Molecular Engineering, Argonne National Laboratory, Lemont, IL 60439, USA.

*Corresponding author. Email: sihongwang@uchicago.edu

cation, low operation voltage, intrinsic compatibility with ion-based biological events, and the possibility of achieving tissue-like stretchability. The sensing function of an OECT is achieved by directly attaching its semiconducting channel to the tissue surface (Fig. 1A), so that a biopotential or targeted biochemical signal can electrostatically modulate the bulk conductivity of the channel (24-27). Because such biosignal transduction is essentially determined by the microscopic distance between the semiconducting channel and a tissue surface (4), neither the conventional periphery fixation through suturing or stapling (Fig. 1B) nor applying a separate adhesive (Fig. 1C) can give the most conformable and stable contact between the semiconducting polymers and tissue surfaces. Instead, the more desired interfacing is to have direct adherence of the semiconducting channel to the tissue surface.

We report the design of a bioadhesive polymer semiconductor (BASC) film that can form robust and rapid adhesion (Fig. 1D) with biotissues under gentle pressure while providing high charge-carrier mobility. This is achieved through a double-network structure formed by a semiconducting polymer and a separate tissue-adhesive polymer. Although there have been reports of tissue-adhesive polymers and hydrogels (28-31), none of these are suitable for the creation of bioadhesive semiconductor films. First, because semiconducting polymers typically have long side chains, it is a challenge to ensure the accessibility of the bioadhesive groups on the film surface. Second, the bioadhesive polymer needs to have coprocessibility with semiconducting polymers that are typically soluble in organic solvents. To achieve good electrical performance, the obtained morphology needs to both keep continuous chargetransport pathways and have only a moderate level of aqueous swellability.

Design of the bioadhesive semiconductor

We designed a brush-architectured bioa sive polymer (BAP) (Fig. 1E) for forming a double-network film with a semiconducting polymer. This bioadhesive polymer has a polyethylene backbone with long linear side chains terminated with two types of functional units in a controlled ratio: carboxylic acid (COOH) and N-hydroxysuccinimide (NHS) ester. The COOH group provides water absorption for temporarily drying the tissue surface and forms electrostatic interactions with tissue surfaces. The NHS ester group, as the primary contributor to bio-adhesion, covalently bonds with the primary amine groups on the tissue surface (28, 29). To allow the effective exposure of these groups on the film surface when blending with a semiconducting polymer, a key innovation in our design is the extension of the side-chain length by inserting tetra(ethylene glycol) (TEG) structure (Fig. 1E). This structure was selected for its moderate level of polarity for providing a suitable level of swelling, which can help to drain the fluid on the tissue surface and facilitate ion transport and, by contrast, will not cause exaggerated swelling and volume expansion.

The semiconductor phase is served by a type of redox-active polymer semiconductor, poly (3,3'-bis(2-(2-methoxyethoxy)ethoxy)-2,2':5',2"-terthiophene) [p(g2T-T); Fig. 1F], which has shown high performance in OECT devices for biosensing functions (32, 33). For the preparation of the double-network film, we blended p(g2T-T) with two types of acrylate monomers (COOH-terminated and NHS esterterminated, respectively) in a controlled ratio (table S2) in chloroform. We then spin-coated the blended solution on a substrate to form thin films and further polymerized and crosslinked the bioadhesive monomers in the films under ultraviolet (UV) light (fig. S1). Such an in situ polymerization process not only solves the cosolubility issue, but also controls the phase separation scale for achieving better percolation connectivity of the p(g2T-T) phase (fig. S2). The obtained bioadhesive semiconductor further enables us to fabricate a fully bioadhesive and stretchable OECT sensor and realize tissueinterfaced sensing (e.g., electrophysiological recording on a wet heart; Fig. 1G) with stable bonding and built-in signal amplification.

Water absorption, morphology, and adhesion properties

According to our hypothesis, when the BASC is in contact with the tissue surface, the brushtype BAP phase starts to absorb and remove water on the tissue surface. To validate this, we first investigated the water absorption and swelling behavior of a neat-brush BAP. After soaking in phosphate-buffered saline (PBS) solution, the mass of BAP increased by ~20% after 2 min from rapid water absorption, which was

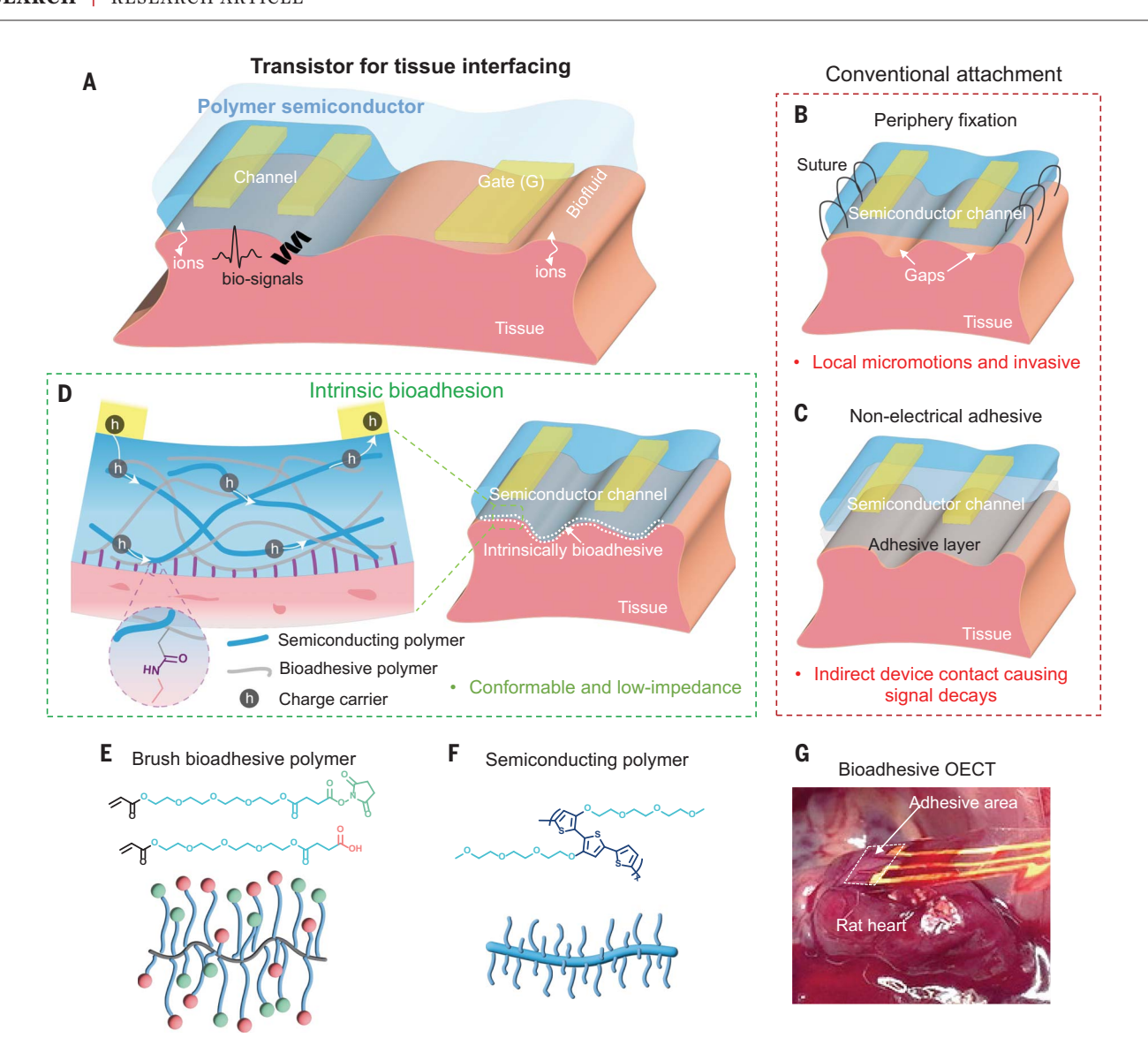


Fig. 1. Bioadhesive polymer semiconductors for electrochemical transistor–based tissue interfacing. (**A**) Use of electrochemical transistors at tissue interfaces for biosensing with built-in amplification, for which biosignals couple into the polymer semiconductor channels through direct tissue contact. (**B** and **C**) Conventional device attachment methods on tissue surfaces, such as peripheral suturing and applying a nonelectrical adhesive layer, and their corresponding limitations. (**D**) Direct adhesive attachment achieved by a BASC channel and a wet tissue surface. The double-network design of the BASC

contains a semiconducting polymer and an adhesive polymer that achieves covalent bonding with tissue surfaces. (\mathbf{E}) Chemical structures of the adhesive monomers with even longer linear side chains terminated with NHS ester and COOH groups, and the schematic of formed BAP. (\mathbf{F}) Chemical structure and a schematic of the utilized polymer semiconductor p(g2T-T) with long linear side chains. (\mathbf{G}) Photograph showing a fully bioadhesive OECT with BASC channel adhered to a rat heart for ECG recording, which can stand for mechanical agitations.

followed by slow absorption over the next 24 hours (Fig. 2A). This was also reflected by the volumetric swelling, which had a lateral expansion ratio of ~1.05 (Fig. 2B). Comparatively, the 1:1 blending of the more hydrophilic COOH group and less hydrophilic NHS ester group renders the BAP with a moderate level of water absorption and swelling, which stands between the levels of the two brush polymers with only COOH- or NHS ester-terminated side chains (BAP-COOH and BAP-NHS, respectively) (fig. S3). The water-absorption behaviors of these three brush-architectured polymers are all much

milder than that of poly(acrylic acid) (PAAc) (fig. S4), which could come from the different film morphologies and porosities (Fig. 2C and fig. S5) of the two different polymer architectures (i.e., brush versus nonbrush) (34, 35). Overall, the moderate level of water absorption for BAP is beneficial for the stability of electrical performance from BASC films.

When the BAP is blended with p(g2T-T) to form BASC films through spin-coating processes, the p(g2T-T) phase self-assembles into interconnected nanofibril structures (Fig. 2E), as evidenced by atomic force microscopy (AFM)

images (Fig. 2D and fig. S6) for the top and bottom surfaces of a film with the blending ratio of 1:40 (in mass) for p(g2T-T)-to-BAP. In the thickness direction, depth-profiling x-ray photoelectron spectroscopy (XPS) showed an increasing fraction of p(g2T-T) from the top to the bottom surface (Fig. 2F). This high ratio of BAP was chosen to ensure sufficient surface density of NHS ester groups for high adhesive property, which we validate further in the next paragraph. Such a dominant amount of BAP in the BASC film also renders the BASC film with similar mechanical properties to BAP, as

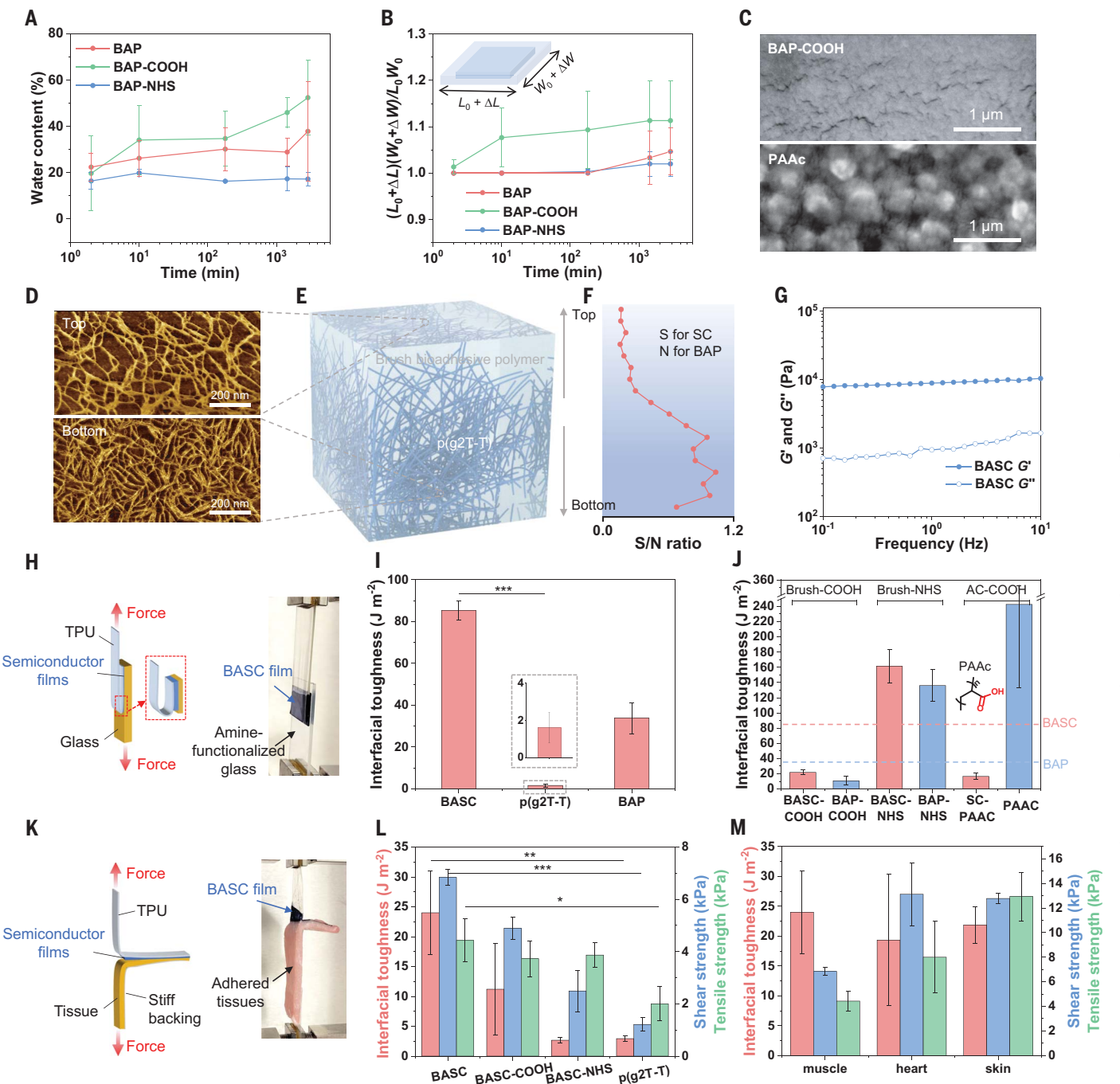


Fig. 2. Adhesive-relevant properties of the BASC films. (A and B) Water content measured through gravimetric analysis (A) and dimensional swelling (B) of the BAPs with three types of side-chain designs when soaked in PBS solution over time. (C) SEM images showing the microscale features of a BAP-COOH film and a PAAc film in the dry state. (D) AFM phase images showing the top and bottom surfaces of a BASC film. (E) Three-dimensional (3D) schematic morphology of a BASC film. (F) XPS-measured ratios between the S element and the N element from the top to the bottom surface of a BASC film. (G) Rheological measurement of the BASC polymer in the dry state. (H) 180° peel test (ASTM D3330) for interfacial toughness measurement on rigid substrates. (I) Interfacial toughness of the adhesion between a BASC film and an amine-functionalized, dry glass substrate, in comparison to a neat p(g2T-T)

film and a BAP film. (**J**) On amine-functionalized glass substrates, interfacial toughness achieved by BASC films and BAP (including PAAc) films with different types of side chains. The two dashed lines mark the levels of interfacial toughness for the BASC and BAP films from (I). (**K**) 180° peel test (ASTM F2256) for interfacial toughness measurement on biotissues. (**L**) Interfacial toughness, shear strength, and tensile strength of the adhesion between wet pig-muscle tissues and a BASC film, a BASC-COOH film, a BASC-NHS film, and a neat p(g2T-T) film, respectively. (**M**) Interfacial toughness, shear strength, and tensile strength achieved by BASC films on various wet tissue surfaces. Values in (I), (J), (L), and (M) represent the mean and the standard deviation (n = 3 independent measurements). Statistical significance and P values are determined by two-sided Student's t test: *P < 0.05, **P < 0.01.

featured by a low modulus and viscoelasticity (Fig. 2G and figs. S7 and S8). These tissue-like mechanical properties are crucial for achieving conformal physical contact with tissue surfaces and further forming adhesion (36).

We next studied the adhesion behavior of BASC films through 180° peel, lap-shear, and tensile tests on various synthetic materials and biotissues, by first holding these films [supported on thermoplastic polyurethane (TPU) substrates] to the different surfaces with gentle pressure (around 5 kPa) for 1 min (fig. S9). On amine-treated glass surfaces, which can form covalent interaction with NHS ester, BASC films displayed much stronger and tougher adhesion than neat p(g2T-T) films with an over 40-fold increase in the interfacial toughness, which achieves even higher level than the BAP film (Fig. 2, H and I, and fig. S10). Tests of BASC films with other blending ratios manifested the general trend of higher adhesion from higher ratios of BAP in the film (fig. S11). On several other synthetic surfaces (i.e., gold, TPU, and PDMS), BASC films also formed much stronger adhesion than neat p(g2T-T) films (fig. S12).

With the side-chain design of the BAP playing the key role in the adhesion property of BASC films, we further compare the BAP (1:1 ratio of COOH and NHS ester) with three polymers with the same backbone but different

side chains: BAP-COOH, BAP-NHS, and regular PAAc. We also made comparisons between the three blended semiconducting films (namely BASC-COOH, BASC-NHS, and SC-PAAc) from each of these polymers with p(g2T-T) in the ratio of 1:40. Through testing on aminefunctionalized glass surfaces, several observations can be made. First, among the three types of brush BAPs and the resulting BASCs, the higher amount of NHS ester gives higher adhesion, which proves that the adhesion is mainly provided by the NHS group. Second, the three BASCs built with the three brush BAPs all provide comparable or higher adhesion properties with their corresponding BAPs. By contrast, the blending of PAAc with p(g2T-T) results in a decrease of adhesion by about 90% (Fig. 2J). This validates our design hypothesis for BAP that states that long side chains are needed for overcoming the shielding effect from the long side chains of p(g2T-T) on the adhesive groups.

We then characterized the adhesion performance of BASC films on wet tissue surfaces (figs. S13 and S14). As shown for pig muscle surfaces, BASC films achieve an interfacial toughness of $^{\rm 24}$ J m $^{\rm -2}$, a shear strength of $^{\rm 7}$ kPa, and a tensile strength of $^{\rm 4.4}$ kPa, which are values that are $^{\rm 10}$ times greater than those of neat p(g2T-T) films for interfacial toughness (Fig. 3, K and L). These adhesion properties are achieved

with an equal ratio of brush COOH and NHSester side chains and are greater than those with COOH- or NHS ester-only side chains (i.e., BASC-COOH and BASC-NHS) (Fig. 2L and fig. S15) or other unbalanced mixing ratios of the two groups (figs. S16 and S17). Such a trend of the side-chain influence is different from the adhesion behaviors on dry amine-glass surfaces, which demonstrates the importance of hydrophilic COOH groups for absorbing water in establishing adhesion on wet tissue surfaces. The BASC film can also be applied to various wet tissues-including the heart, skin, and spleenwith high interfacial toughness, high shear strength, and high tensile strength (Fig. 2M and fig. S15).

Electrical performance in OECT devices

Designed as a semiconductor, the electrical performance of BASC films was characterized in OECT devices (Fig. 3A). The OECT's transfer curve with an on/off ratio of 10^4 indicates ideal semiconducting performance from the BASC film (Fig. 3B and fig. S18), which is on par with that of p(g2T-T). As calculated from the transconductance ($g_{\rm m}$), the obtained charge-carrier mobility of the BASC film approaches $1~{\rm cm}^2~{\rm V}^{-1}~{\rm s}^{-1}$, which is comparable to that of the neat p(g2T-T) film (Fig. 3C and figs. S19 and S20). This is given by the percolated charge-transport pathway formed by the p(g2T-T) phase in the

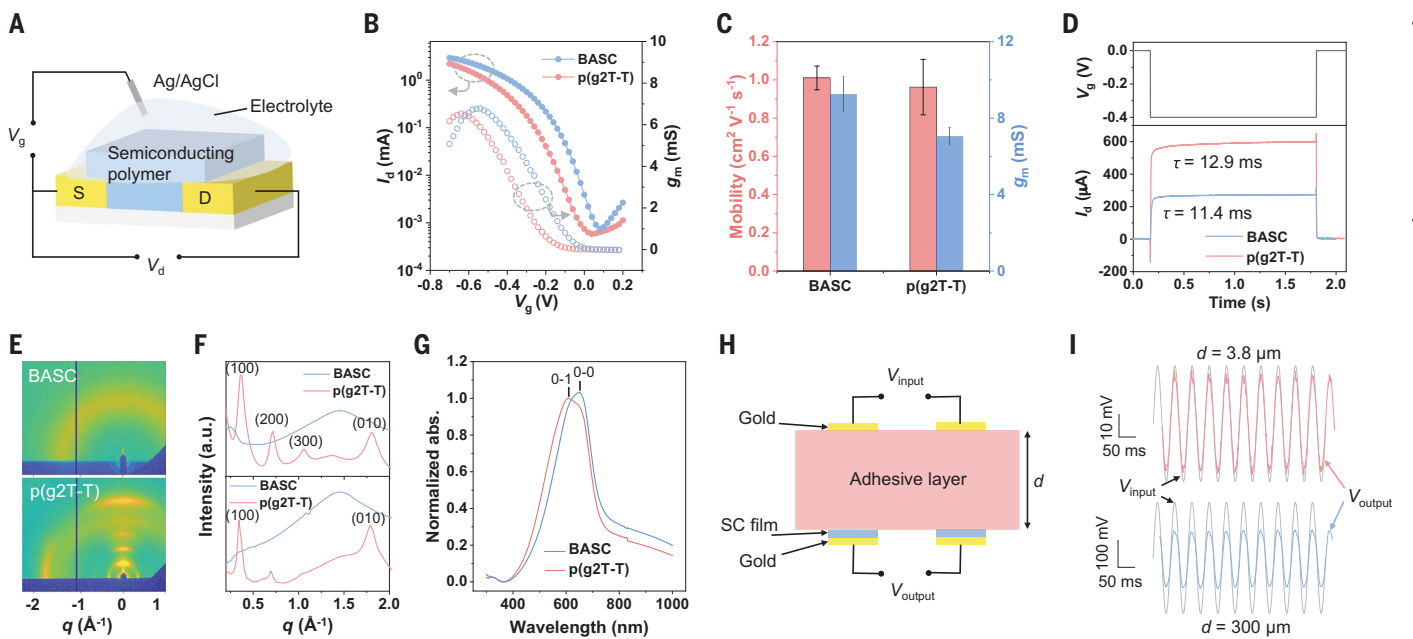


Fig. 3. Electrical and structural characterizations of the BASC film. (**A**) Setup for the OECT-based characterizations. (**B**) Transfer curves from a BASC film and a p(g2T-T) film serving as the OECT channel. V_g , gate voltage; I_d , drain current; V_d , drain voltage; g_m , transconductance. (**C**) Charge-carrier mobility and g_m for the BASC and p(g2T-T) films. Values represent the mean and the standard deviation (n = 5 independent measurements). (**D**) Response-speed measurement with applied gate-voltage pulse and drain-current response. (**E**) 2D GIXD patterns of the BASC and p(g2T-T) films. (**F**) 1D linecuts in the out-of-plane

direction (top) and in-plane direction (bottom) of a BASC and a p(g2T-T) film. a.u., arbitrary units. (**G**) Normalized UV-vis absorption of a BASC and a p(g2T-T) film. (**H**) Schematic diagram showing the setup for characterizing the influence of the device-tissue distance caused by the use of a separate bioadhesive layer. (**I**) AC signal input (gray) and acquired signals between the p(g2T-T) electrodes that are covered with a layer of BAP with two different thicknesses. The thin adhesive layer (thickness, $d = 3.8 \,\mu\text{m}$) decreases the signal amplitude by 15% whereas the thick adhesive layer ($d = 300 \,\mu\text{m}$) decreases the amplitude by 50%.

BASC film. On the device level, the maximum transconductance (i.e., the key figure-of-merit for OECT performance) of the BASC film displays a slight increase compared with the p(g2T-T) film (Fig. 3C), which should result from the much greater thickness (1.9 μ m) of the BASC film compared with that (35 nm) of the neat p(g2T-T)

film. In the meantime, the measurement of the OECT response speed of these semiconducting films shows that the higher thickness of the BASC film does not lead to a slower response to the gating compared with the neat p(g2T-T) film (Fig. 3D), as ions can transport very efficiently in the blended BAP.

We carried out grazing-incidence x-ray diffraction (GIXD) and UV-visible (UV-vis) spectroscopy (Fig. 3G and fig. S21) to study interchain packing morphology of the p(g2T-T) phase in the film. The GIXD results (Fig. 3, E and F) show that blending with the brush-architected BAP almost completely suppresses the long-range

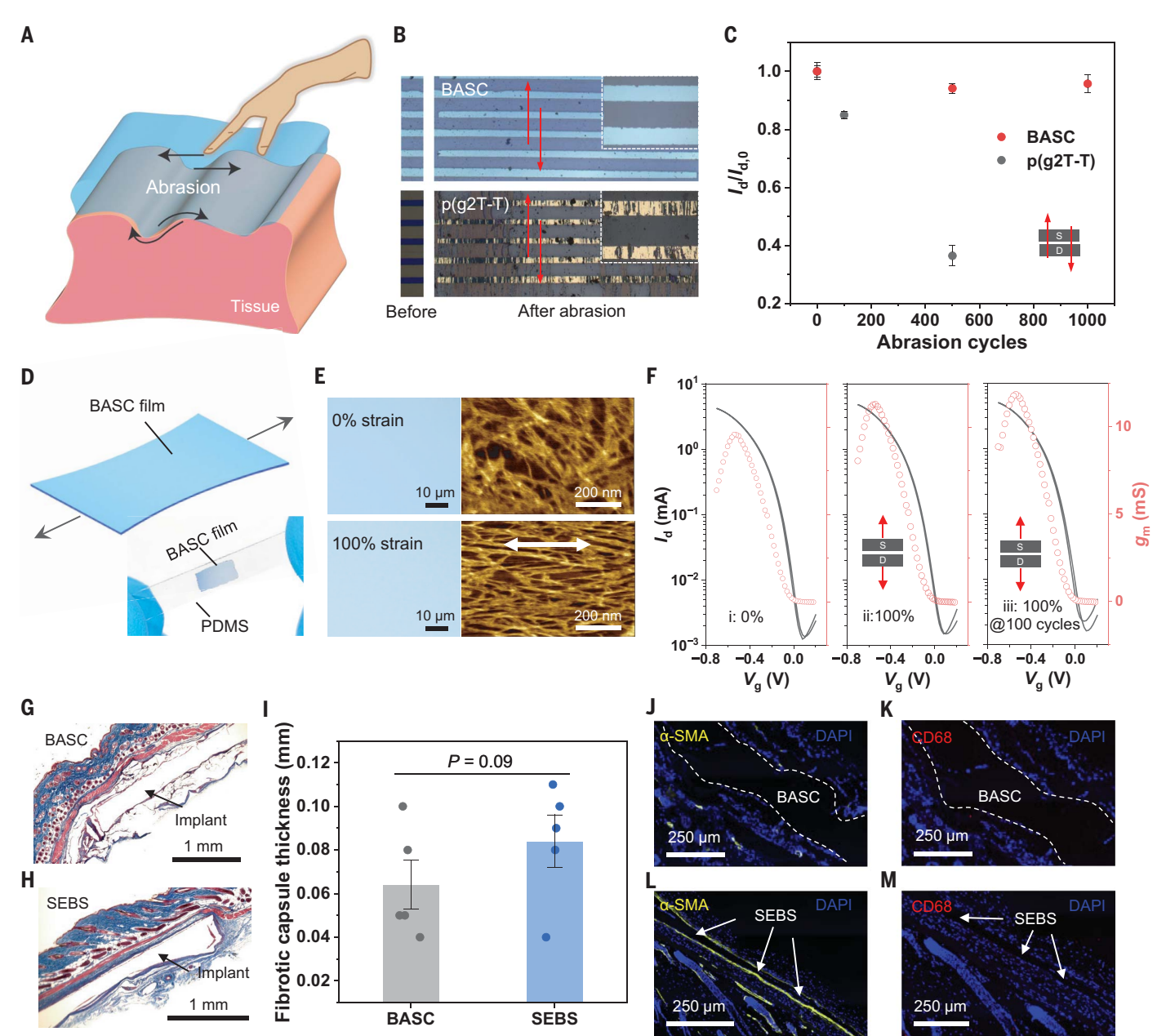


Fig. 4. Abrasion resistance, stretchability, and biocompatibility of BASC films. (A) Schematic diagram illustrating physical abrasions that can happen on the surfaces of implantable devices. **(B)** Photographs showing a BASC film and a p(g2T-T) film before and after abrasion by a PTFE-covered glass plate under 1 kPa for 500 cycles. The arrows indicate the direction of the abrasion. **(C)** Changes of OECT on current from the two films after the abrasion cycles along the charge-transport direction. Values represent the mean and the standard deviation (n = 4 or 5 independent measurements). **(D)** Schematic that illustrates a BASC film under stretching. The bottom photograph shows a stretched BASC film on a PDMS substrate at 100% strain. **(E)** Optical

microscopy and AFM images showing a BASC film stretched to 100% strain without forming cracks. (**F**) Transfer curves of BASC films in the pristine state and stretched to 100% strain for 1 and 100 cycles, which were measured with $V_d = -0.6$ V. (**G** and **H**) Masson's trichrome staining of surrounded tissues of a subcutaneously implanted BASC film (G) and a SEBS film (control) (H) after one month in mice. (**I**) Calculated fibrotic-capsule thickness. (**J** to **M**) Immunofluorescence staining of α -SMA for fibroblasts (yellow) [(J) and (L)] and CD68 for macrophages (red) [(K) and (M)]. Statistical significance and P values are determined by two-sided Student's t test: ns, not significant; **P < 0.01.

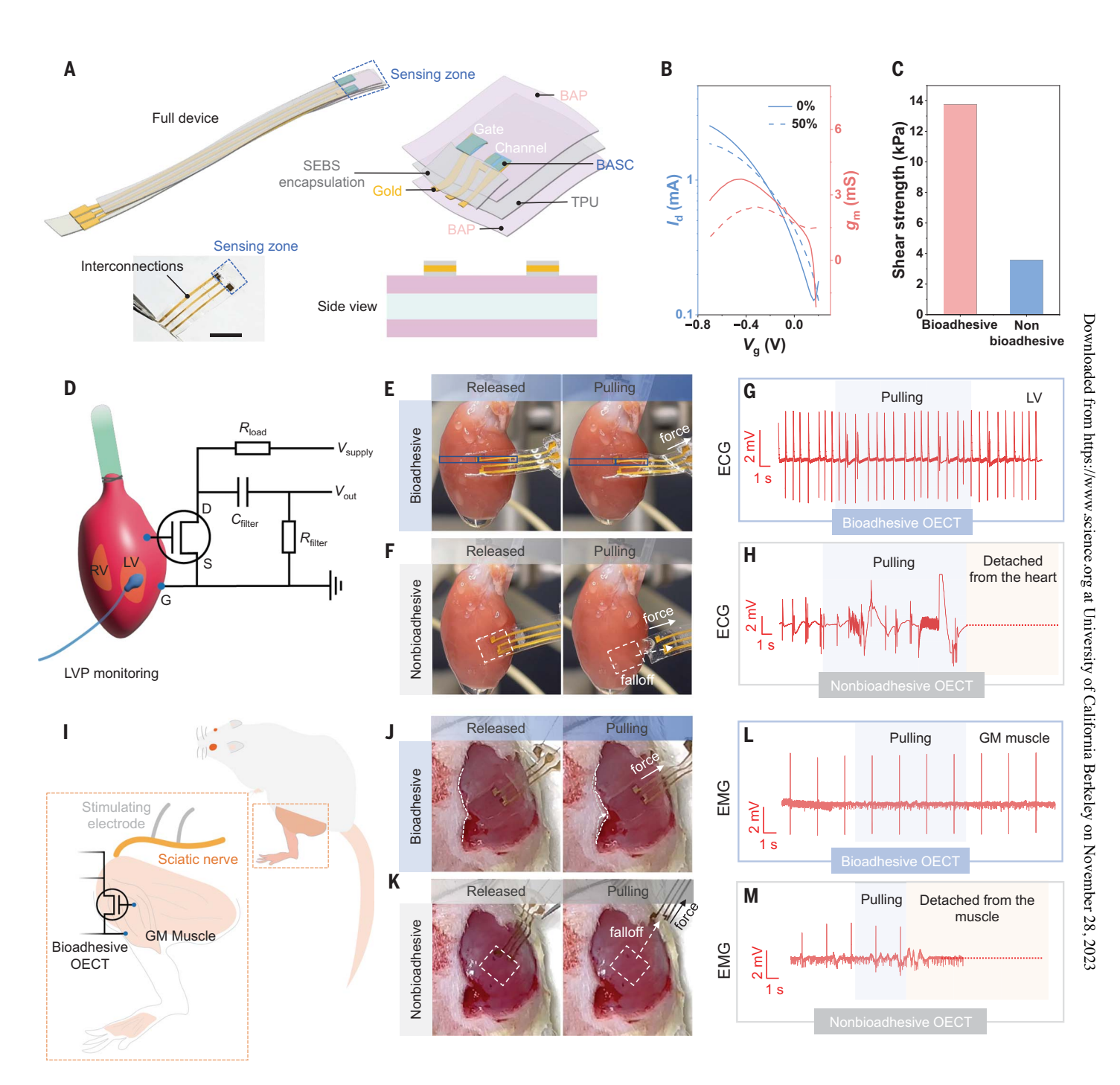


Fig. 5. Fully bioadhesive OECT sensor and the use for ex vivo and in vivo electrophysiological recording. (**A**) Device structure and picture. Scale bar, 5 mm. (**B**) Transfer curves for a fully bioadhesive OECT under 0 and 50% strains. (**C**) Shear strength of the adhesion between a fully bioadhesive OECT on the pig muscle tissue, in comparison to an OECT with nonbioadhesive surface. (**D**) Schematic that shows the use of the OECT sensor for ECG recording on a heart surface and the circuit diagram. LVP, left ventricular pressure; *G*, gate electrode; *D*, drain electrode; *S*, source electrode; *R*, resistor; *C*, capacitor. (**E**) Photographs that show a fully bioadhesive OECT attached to an isolated rat-heart surface maintaining stable contact during mechanical agitation. (**F**) Comparison with a nonbioadhesive OECT, for which capillary-based attachment cannot maintain

conformable and stable contact. (\mathbf{G}) ECG signals recorded by the fully bioadhesive OECT on the LV. (\mathbf{H}) ECG recording by the nonbioadhesive OECT, which ceased after the device detached from the heart. (\mathbf{I}) Schematic that shows the use of the OECT sensor for EMG recording on the GM muscles upon stimulation of the sciatic nerve. (\mathbf{J}) Photographs that show a fully bioadhesive OECT attached to the GM muscle maintaining stable contact during mechanical agitation. (\mathbf{K}) Comparison with a nonbioadhesive OECT, for which capillary-based attachment cannot maintain conformable and stable contact. (\mathbf{L}) EMG signals recorded by the fully bioadhesive OECT on the GM muscle. (\mathbf{M}) EMG signals recorded by the nonbioadhesive OECT on the GM muscle, which ceased after the device detached from the muscles.

Li et al., Science **381**, 686-693 (2023) 11 August 2023 **6 of 8**

crystallization, which could decrease the modulus of the p(g2T-T) phase. However, the UV-vis absorption spectroscopies show that the p(g2T-T) phase in the BASC film has a higher level of short-range aggregation than the neat film, which is represented by the ratios between 0-0 and 0-1 optical transition peaks (Fig. 3G). At the molecular level, this explains the well-maintained mobility from the BASC film.

For the direct interfacing of a semiconducting polymer with a biotissue surface for sensing biophysical or biochemical signals, the other two important interface factors that influence the recorded signal amplitudes are interfacial impedance and the separation distance between the recording and tissue surfaces. For the interfacial impedance, electrochemical impedance spectroscopy (EIS) measurements do show that our double-network BASC design gives lower impedance than applying a separate adhesive at the interface (figs. S22 to S24). Our BASC design helps to keep the closest distance between the semiconducting film and the tissue surface during recording. To semiquantitatively assess the effect of using separate adhesion layers in increasing the distance between the device and tissue surfaces (37-40), we coated our BAP polymer in two different thicknesses (3.8 and 300 µm) onto a pair of p(g2T-T)-based recording electrodes (Fig. 3H). This layout emulates the channel and the gate in OECT devices. To show the recording capability, we applied alternating current (AC) signals through another pair of gold electrodes that are attached to the top surface of the BAP coating layer, which was fully soaked with PBS solution. Increasing the thickness of the BAP layers from 3.8 to 300 μm led to substantial decreases in the potential sensed between the two p(g2T-T) electrodes (Fig. 3I), which shows major signal decay caused by the use of a separate adhesive layer.

Abrasion resistance, stretchability, and biocompatibility

When a polymer semiconductor is interfaced with biotissues, several other properties, including abrasion resistance, stretchability, and biocompatibility, are important to the robustness and long-term stability of the interface and the function. During insertion and/or attachment of a device into or onto biotissues, physical abrasion can occur on the device surface (Fig. 4A). With conjugated polymers typically having relatively low stretchability and toughness, the films are generally susceptible to abrasions (41). Our BASC film shows abrasion resistance, which should come from the ultrasoft and viscoelastic properties (fig. S26) of the film. To characterize this, we used a piece of polytetrafluoroethylene (PTFE)-covered glass to slide back and forth on a BASC film under a pressure of 1 kPa. After 1000 cycles of such surface sliding, the BASC film remained mostly intact in appearance under an optical microscope and electrical performance in an OECT device (Fig. 4, B and C). By comparison, a neat p(g2T-T) film was damaged by the surface abrasion processes. To better mimic the abrasion during device implantation processes, we also carried out the comparison using pig skin, which gives a similar trend (fig. S25). The brief tissue contact during typical abrasion processes would not be sufficient for BASC films to generate adhesion with the tissue surfaces and further create higher frictional force.

As both p(g2T-T) and the BAP gel are highly stretchable (10), the resulting BASC films also have high stretchability (Fig. 4D), which benefits conformability to curvilinear tissue surfaces and robustness under tissue deformations. From the optical microscopy and AFM images, the BASC film can be stretched to 100% strain without forming any cracks (Fig. 4E). Instead, we observed strain-induced alignment of the p(g2T-T) nanofibers. When tested in OECT devices, the BASC film displayed highly stable electrical performance during stretching to 100% strain, even after 100 repeated cycles (Fig. 4F and fig. S27).

When a device is interfaced with tissue, the foreign-body response (FBR) is one of the main factors that limit the longevity (42, 43), which is influenced by the modulus and the surface chemistry of an implant. We studied this behavior of our BASC films by laminating them on both sides of SEBS [polystyrene-block-poly (ethylene-ran-butylene)-block-polystyrene] substrates and implanting them subcutaneously in mice. After one month of implantation, the fibrotic capsules that formed around the BASC samples are thinner than those formed around SEBS control samples, which is shown by Masson's trichrome staining results (Fig. 4, G to I). Additionally, immunofluorescence imaging of FBR-related biomarkers (i.e., α -SMA and CD68) shows lower amounts of fibroblasts and macrophages deposited on the BASC surface than those on the SEBS samples (Fig. 4, J to M). These results collectively show that BASC films have better biocompatibility than SEBS, which further elevates the promise for directly interfacing with biotissues through implantable devices. In addition, in vitro cell culture (fig. S28) confirms minimal cytotoxicity of the films.

Fully bioadhesive OECT sensor for ex vivo and in vivo electrophysiological recording

We designed and fabricated an OECT-based sensor (Fig. 5A and fig. S29) using BASC films as both the semiconducting channel and the redox-active gate. The surrounding area is occupied by the substrate, which is covered by our BAP film. With the use of microcrack-based stretchable gold (figs. S30 and S31) as the electrodes (44, 45) and thin SEBS layers (~570 nm thick) as the encapsulation for the interconnects and the bottom side of the elec-

trodes, the OECT sensor is also stretchable. An as-fabricated fully bioadhesive OECT displays ideal transfer behavior at 0% strain and when stretched to 50% strain (Fig. 5B and fig. S32) and forms strong adhesion when attached to the surface of a wet pig muscle (Fig. 5C).

We further demonstrated the benefit of the bioadhesive property of the OECT sensor on an epicardial electrocardiogram (ECG) recording from an isolated rat heart (Fig. 5D). The bioadhesive OECT can be conveniently adhered to the wet heart surface by gently pressing for 20 s. During the recording process, the bioadhesive and stretchable properties working in conjunction helped the OECT to well accommodate the heart beating, thereby maintaining spatially stable and conformable contact on the heart (Fig. 5E, fig. S34, and movie S1). Even under external mechanical perturbation (e.g., pulling), stable attachment was still maintained. The ECG recording from both the left ventricle (LV) and right ventricle (RV) surfaces also remained stable (Fig. 5G and fig. S34). By comparison, for a nonbioadhesive OECT (figs. S35 and S36), which can only stay on the heart surface by means of capillary force from the fluid, gradual drifting and complete detachment can happen as a result of either heart beating or external perturbation (e.g., pulling) (Fig. 5F, fig. S34, and movie S2). This substantially affects the quality and stability of ECG recording (Fig. 5H).

We also demonstrated the in vivo use of the bioadhesive OECT on an under-skin electromyogram (EMG) recording from the gastrocnemius medialis (GM) muscle of a live rat, for which the OECT can also form stable adhesion by gentle pressing (Fig. 5I and fig. S37). During electrical stimulation of the sciatic nerve for triggering leg movements, EMG signals corresponding to each stimulation can be stably recorded without being affected by mechanical perturbation (e.g., pulling) (Fig. 5, J and L, and movie S3), which is in stark contrast with the nonbioadhesive OECT (Fig. 5, K and M, and movie S4). Furthermore, we also validated the benefits of such direct tissue adhesion as compared with suturing (fig. S38) or a separate adhesive layer (fig. S39) in low invasiveness and/or higher signal amplitude and stability. Such benefits couple with the built-in amplification ability of OECT-based active sensor [illustrated by the comparison with a poly(3,4-ethylenedioxythiophene) polystyrene sulfonate (PEDOT:PSS)-based passive recording device; fig. S40].

REFERENCES AND NOTES

- S.-H. Sunwoo, K.-H. Ha, S. Lee, N. Lu, D.-H. Kim, Annu. Rev. Chem. Biomol. Eng. 12, 359–391 (2021).
- 2. H. Yuk, B. Lu, X. Zhao, Chem. Soc. Rev. 48, 1642-1667 (2019).
- 3. I. You et al., Science 370, 961-965 (2020).
- J. Rivnay, H. Wang, L. Fenno, K. Deisseroth, G. G. Malliaras, Sci. Adv. 3, e1601649 (2017).
- 5. S. Liu, Y. Rao, H. Jang, P. Tan, N. Lu, Matter 5, 1104-1136 (2022).
- 6. H. Yuk, J. Wu, X. Zhao, *Nat. Rev. Mater.* **7**, 935–952 (2022).
- 7. J. Xu et al., Science **355**, 59-64 (2017).
- 8. S. Wang et al., Nature 555, 83-88 (2018).

Li et al., Science 381, 686-693 (2023) 11 August 2023 7 of 8

- 9. Y. Jiang et al., Science 375, 1411-1417 (2022).
- 10. Y. Dai et al., Adv. Mater. 34, e2201178 (2022).
- 11. Z. Yan et al., Science 375, 852-859 (2022).
- 12. K. Sim et al., Nat. Electron. 3, 775-784 (2020)
- 13. Q. Yang et al., Nat. Mater. 20, 1559-1570 (2021).
- 14. X. Wang et al., Matter 5, 1204-1223 (2022).
- 15. I. K. Han et al., Adv. Mater. 35, 2203431 (2022)
- 16. J. Deng et al., Nat. Mater. 20, 229-236 (2021).
- S. Li, Y. Cong, J. Fu, J. Mater. Chem. B Mater. Biol. Med. 9, 4423–4443 (2021).
- 18. F. Torricelli et al., Nat. Rev. Methods Primers 1, 66 (2021).
- A. Marks, S. Griggs, N. Gasparini, M. Moser, Adv. Mater. Interfaces 9, 2102039 (2022).
- 20. J. Rivnay et al., Nat. Rev. Mater. 3, 17086 (2018).
- B. D. Paulsen, K. Tybrandt, E. Stavrinidou, J. Rivnay, *Nat. Mater.* 19, 13–26 (2020).
- 22. J. Chen et al., Nat. Mater. 21, 564-571 (2022)
- 23. Y. Jimbo et al., Proc. Natl. Acad. Sci. U.S.A. 118, e2022300118 (2021).
- G. D. Spyropoulos, J. N. Gelinas, D. Khodagholy, Sci. Adv. 5, eaau7378 (2019).
- 25. C. Cea et al., Nat. Mater. 19, 679-686 (2020).
- 26. S. L. Bidinger et al., Sci. Adv. 8, eadd4111 (2022)
- 27. K. Guo et al., Nat. Biomed. Eng. 5, 666-677 (2021).
- 28. J. Li et al., Science 357, 378-381 (2017).
- 29. H. Yuk et al., Nature 575, 169-174 (2019)
- 30. B. Xue et al., Nat. Commun. 12, 7156 (2021).
- 31. Z. Ma et al., Science 377, 751-755 (2022).
- 32. C. B. Nielsen et al., J. Am. Chem. Soc. 138, 10252-10259 (2016).
- 33. S. Inal, G. G. Malliaras, J. Rivnay, Nat. Commun. 8, 1767 (2017).
- 34. M. Zhang, A. H. E. Müller, *J. Polym. Sci. A Polym. Chem.* **43**, 3461–3481 (2005).
- 35. E. Dashtimoghadam et al., Nat. Commun. 12, 3961 (2021).
- 36. C. M. Tringides et al., Nat. Nanotechnol. 16, 1019–1029 (2021).

- 37. A. H. Marblestone et al., Front. Comput. Neurosci. 7, 137 (2013).
- 38. J. Du et al., J. Neurophysiol. 101, 1671–1678 (2009).
- 39. O. Herreras, Front. Neural Circuits 10, 101 (2016).
- N. Pérez-Prieto, M. Delgado-Restituto, Front. Neurosci. 15, 681085 (2021).
- A. X. Chen, A. T. Kleinschmidt, K. Choudhary, D. J. Lipomi, Chem. Mater. 32, 7582–7601 (2020).
- S. Capuani, G. Malgir, C. Y. X. Chua, A. Grattoni, Bioeng. Transl. Med. 7. e10300 (2022).
- R. Biran, D. C. Martin, P. A. Tresco, Exp. Neurol. 195, 115–126 (2005).
- N. Matsuhisa, X. Chen, Z. Bao, T. Someya, Chem. Soc. Rev. 48, 2946–2966 (2019).
- 45. Y. Lee et al., Sci. Adv. 7, eabg9180 (2021).

ACKNOWLEDGMENTS

We thank the University of Chicago Animal Resources Center (RRID:SCR_021806), especially A. Solanki for his assistance with animal surgery and housing. All the animal experiments performed in this research were approved by the Institutional Animal Care and Use Committee of the University of Chicago under the protocols of ACUP 72378 and ACUP 72450. Funding: This work was supported by the National Science Foundation (NSF) (award no. 2105367), the US National Institutes of Health Director's New Innovator Award (1DP2EB034563), and the US Office of Naval Research (N00014-21-1-2266 and N00014-21-1-2581). This work was partially supported by the University of Chicago Materials Research Science and Engineering Center (which is funded by the NSF under award no. DMR-2011854) and the start-up fund from the University of Chicago. This work used the Soft Matter Characterization Facility (SMCF) at the University of Chicago. This research used resources of the Advanced Photon Source. a US Department of Energy (DOE) Office of Science user facility

operated for the DOE Office of Science by Argonne National Laboratory under contract no. DE-ACO2-06CH11357. Y.W. and X.G. thank the financial aid from NSF grant DMR-2047689. Author contributions: S.Wang conceived of and supervised this research. N.L. and S.Wang designed the experiments. N.L. and N.S. synthesized and characterized the monomers and polymers. N.L. and Y.Li performed the mechanical tests. N.L., Y.Li, Y.Liu, Y.D., S.L., and A.Z. fabricated the transistor devices and performed the measurements. N.L., Y.D., and J.S. performed the GIXD characterization. Z.C., N.L., and B.T. performed the ex vivo ECG and in vivo EMG measurements. S.K., N.L., S.Wai, and J.A.H. performed the biocompatibility study. Y.W. and X.G. conducted the film-on-water test. W.L. and C.Z. participated in the discussions. N.L. and S.Wang cowrote the paper. All authors reviewed and commented on the manuscript. Competing interests: S.Wang and N.L. are inventors on patent application no. UCHI 23-T-101 submitted by the University of Chicago. Data and materials availability: All data are available in the manuscript or the supplementary materials. License information: Copyright © 2023 the authors, some rights reserved; exclusive licensee American Association for the Advancement of Science. No claim to original US government works. https://www.science.org/about/science-licenses-journal-article-reuse

SUPPLEMENTARY MATERIALS

science.org/doi/10.1126/science.adg8758 Materials and Methods Figs. S1 to S40 Tables S1 to S4 References (46–72) MDAR Reproducibility Checklist Movies S1 to S4

Submitted 26 January 2023; accepted 14 June 2023 10.1126/science.adg8758

Li et al., Science 381, 686-693 (2023) 11 August 2023 8 of 8



Bioadhesive polymer semiconductors and transistors for intimate biointerfaces

Nan Li, Yang Li, Zhe Cheng, Youdi Liu, Yahao Dai, Seounghun Kang, Songsong Li, Naisong Shan, Shinya Wai, Aidan Ziaja, Yunfei Wang, Joseph Strzalka, Wei Liu, Cheng Zhang, Xiaodan Gu, Jeffrey A. Hubbell, Bozhi Tian, and Sihong Wang

Science 381 (6658), . DOI: 10.1126/science.adg8758

Editor's summary

Bioelectronic devices can be used to monitor or repair vital tissues in the body, but this often requires direct interfacing and adhesion, which is a particular challenge when the surface is wet. Li *et al.* designed a double-network copolymer that combines a bioadhesive with a semiconductor (see the Perspective by Wu and Zhao). In particular, the brush component included a side group that could absorb water so that on initial contact with the tissue surface, it helps to dry it to enhance adhesion. The authors demonstrate the capabilities of their material by building a sensor for electrophysiological recording on an isolated rat heart and on in vivo rat muscles. —Marc S. Lavine

View the article online

https://www.science.org/doi/10.1126/science.adg8758

Permissions

https://www.science.org/help/reprints-and-permissions

Use of this article is subject to the Terms of service